Quantitative analysis of a frequency-domain nonlinearity indicator

Brent O. Reichman,[a] Kent L. Gee, Tracianne B. Neilsen, and Kyle G. Miller
Department of Physics and Astronomy, Brigham Young University, Provo, Utah 84602, USA

(Received 20 March 2015; revised 8 October 2015; accepted 29 March 2016; published online 9 May 2016)

In this paper, quantitative understanding of a frequency-domain nonlinearity indicator is developed. The indicator is derived from an ensemble-averaged, frequency-domain version of the generalized Burgers equation, which can be rearranged in order to directly compare the effects of nonlinearity, absorption, and geometric spreading on the pressure spectrum level with frequency and distance. The nonlinear effect is calculated using pressure-squared-pressure quadspectrum. Further theoretical development has given an expression for the role of the normalized quadspectrum, referred to as Q/S by Morfey and Howell [AIAA J. **19**, 986–992 (1981)], in the spatial rate of change of the pressure spectrum level. To explore this finding, an investigation of the change in level for initial sinusoids propagating as plane waves through inviscid and thermoviscous media has been conducted. The decibel change with distance, calculated through Q/S, captures the growth and decay of the harmonics and indicates that the most significant changes in level occur prior to sawtooth formation. At large distances, the inviscid case results in a spatial rate of change that is uniform across all harmonics. For thermoviscous media, large positive nonlinear gains are observed but offset by absorption, which leads to a greater overall negative spatial rate of change for higher harmonics. © *2016 Acoustical Society of America*.
[http://dx.doi.org/10.1121/1.4945787]

[JFL] Pages: 2505–2513

I. INTRODUCTION

The use of signal processing metrics as indicators of nonlinear propagation has been largely motivated by analysis of high-amplitude noise from launch vehicles,[1–3] military jet aircraft,[4–7] and laboratory-scale jets.[8–14] Some *ad hoc* statistical measures have been used, such as scatterplots of the time rate of increase versus the magnitude of the pressure rise,[1,2] wave or average steepening factors[8,13,15] or the skewness of the pressure time derivative,[3,5,7,12] for which changes as a function of source conditions, distance, or angle have yielded insights regarding nonlinearity. However, more quantitative interpretations of the average steepening factor[16] and the derivative skewness[17] have been provided by examining how the measures evolve for analytical nonlinear propagation scenarios.

While these *ad hoc* indicators can be leveraged to obtain significant physical insight, other nonlinearity indicators have been motivated directly from the generalized Burgers equation (GBE): a parabolic approximation to the second-order wave equation that incorporates the effects of cumulative quadratic nonlinearity, absorption and dispersion, and geometric spreading. Manipulation and ensemble-averaging of the frequency-domain GBE has resulted in two related higher-order spectral quantities that can be leveraged as nonlinearity indicators. The first is the bispectrum, a two-dimensional higher-order spectrum[18] that has been used in, e.g., the physical sciences, engineering, and economics to examine time series for non-Gaussianity and quadratic nonlinearity, but which was tied explicitly to the GBE by Gurbatov *et al.*[19,20] The bispectrum has been used to analyze one-dimensional noise propagation[21] and jet noise.[22,23] Gagnon[24] has provided additional discussion and insights.

The second measure, which forms the subject of the current work, stems from the imaginary part of the cross-spectral density between the pressure and squared-pressure waveforms,[25,26]

$$Q_{pp^2}(\omega) = \mathrm{Im}\left\{\lim_{T\to\infty}\frac{1}{T}E\left[\mathcal{F}^*\{p(t)\}\mathcal{F}\{p^2(t)\}\right]\right\}. \quad (1)$$

Definitions for the Fourier transform and expectation value may be found in many sources; this paper will follow the conventions found in Bendat and Piersol.[27] Its connection to the GBE was first shown by Morfey and Howell,[28] who were seeking a model equation for the nonlinearly evolving power spectral density. They discussed how although $Q_{pp^2}(w)$ was not useful as a long-range predictor of spectral evolution, a normalized quadspectral density, dubbed Q/S, could be useful as a nonlinearity indicator. Note that despite the attention that the Morfey and Howell[28] work has received in the context of aeroacoustic data analysis, it was actually Nagata[29,30] who introduced the pressure-squared-pressure cross spectrum as the Fourier transform of a third-order covariance function in the context of non-Gaussian ocean data analysis. He further showed its explicit mathematical relationship to the bispectrum, a relationship that was later reinforced by Gurbatov *et al.*[19,20] in the context of the GBE.

[a]Electronic mail: brent.reichman@gmail.com

Since the work of Morfey and Howell,[28] the quantity Q/S has been used in several situations to show the effects of nonlinearity. McInerny was among the first to apply the indicator, using it to point to the presence of nonlinearity in rocket noise[2] and military jet flyovers.[31] Similarly, Gee *et al.*[6] used Q/S as evidence for nonlinear propagation in F/A-18E ground run-up data, and the quadspectrum has also been investigated for model-scale jets.[9,32] Other uses range from combustion noise in rocket engines[33] to examining evidence of nonlinearity in legacy commercial aircraft noise.[34] Falco,[35] Falco *et al.*,[36] and Falco *et al.*[37] investigated different forms of the quadspectrum and its meaning for one-dimensional propagation, including the development of a spectral Gol'dberg number.

Despite usage of the pressure-squared-pressure quadspectrum as reviewed above, a quantitative interpretation of the analysis measure has been elusive. Because of the limitations of Q/S in predictive schemes[28] and its difficulty in interpretation,[35] some have questioned its usefulness.[13] The purpose of this paper is to show that by further manipulating the frequency-domain ensemble-average version of the GBE, the spatial rate of change in pressure spectrum level may be expressed as a sum of three individual terms, representing geometric spreading, atmospheric absorption, and nonlinearity. First, the derivation of the ensemble-averaged, frequency domain version of the GBE is presented, followed by further derivations to show how the spatial rate of change in pressure spectrum level may be calculated with Q/S. Changes in the pressure spectrum level predicted using waveform quadspectral analysis are then compared with changes calculated directly from two analytical solutions to the GBE: the Blackstock Bridging Function and the Mendousse Solution. These comparisons show that Q/S can be used as a single-point quantifier of second-order cumulative nonlinear propagation.

II. DERIVATION

In this section, a derivation of the ensemble-averaged GBE is presented, similar to Ref. 28, and extended to yield an expression for the spatial rate of change of the sound level as a sum of the changes due independently to geometric spreading, atmospheric absorption, and nonlinearity. Additionally, the special case of a planar, initially sinusoidal waveform is considered. These developments lay the foundation for quantifying the rate of change in pressure spectrum level with range due to nonlinearity.

A. The spectral GBE

The GBE for an arbitrarily diverging pressure waveform, $p(t)$, in thermoviscous media may be written as

$$\frac{\partial p}{\partial r}+\frac{m}{r}p-\frac{\delta}{2c_0^3}\frac{\partial^2 p}{\partial \tau^2}=\frac{\beta p}{\rho_0 c_0^3}\frac{\partial p}{\partial t}, \tag{2}$$

where δ is the diffusivity of sound; β is the coefficient of nonlinearity; c_0 is the speed of sound; ρ_0 is the equilibrium density of sound; $m=0$, 0.5, or 1 for planar, cylindrical, or spherical waves, respectively; τ is retarded time, and r is the distance from the source. A Fourier transform of Eq. (2) produces the frequency domain GBE:

$$\frac{\partial \tilde{p}}{\partial r}+\frac{m}{r}\tilde{p}+\frac{\omega^2\delta}{2c_0^3}\tilde{p}=\frac{i}{2}\frac{\beta}{\rho_0 c_0^3}\omega\tilde{q}, \tag{3}$$

where $\sim$ denotes a complex Fourier spectrum, and $\tilde{q}$ is the Fourier transform of $p^2(\tau)$. Multiplication of Eq. (3) by r^m and simplification yields

$$\left(\frac{\partial}{\partial r}+\frac{\omega^2\delta}{2c_0^3}\right)r^m\tilde{p}=\frac{i}{2}\frac{\beta}{\rho_0 c_0^3}\omega r^m\tilde{q}. \tag{4}$$

Though the GBE in Eq. (2) is developed for thermoviscous media, it can be modified to include arbitrary absorption and dispersion.[38] This is accomplished by replacing $\omega^2\delta/2\,c_0^3$ in Eq. (3) with α', a combination of the linear attenuation and dispersion coefficients for progressive plane waves, which results in

$$\left(\frac{\partial}{\partial r}+\alpha'\right)r^m\tilde{p}=\frac{i}{2}\frac{\beta\omega}{\rho_0 c_0^3}r^m\tilde{q}. \tag{5}$$

Equation (5) is identical to Eq. (3) in Morfey and Howell[28] for spherical spreading ($m=1$) and is valid for a weakly nonlinear ($|p|\ll\rho_0 c_0^2$) deterministic spherical wave in the far field, with weak attenuation and dispersion present ($|\alpha'|\ll\omega/c_0$). Multiplication of both sides of Eq. (5) by $r^m\tilde{p}*$ yields

$$r^m\tilde{p}^*\left(\frac{\partial}{\partial r}+\alpha'\right)r^m\tilde{p}=\frac{i}{2}\frac{\beta\omega}{\rho_0 c_0^3}r^{2m}\tilde{p}^*\tilde{q}. \tag{6}$$

The real part of Eq. (6) may be simplified as

$$\frac{1}{2}\frac{\partial}{\partial r}\left(r^{2m}\tilde{p}^*\tilde{p}\right)+\alpha r^{2m}\tilde{p}^*\tilde{p}=-\frac{1}{2}\frac{\beta\omega}{\rho_0 c_0^3}r^{2m}\mathrm{Im}\{\tilde{p}^*\tilde{q}\}, \tag{7}$$

where $\alpha=\mathrm{Re}\{\alpha'\}$ is the linear absorption coefficient. Ensemble averaging of Eq. (7) gives

$$\frac{1}{2}\frac{\partial}{\partial r}\left(r^{2m}S_{pp}\right)+\alpha r^{2m}S_{pp}=-\frac{1}{2}\frac{\beta\omega}{\rho_0 c_0^3}r^{2m}Q_{pp^2}, \tag{8}$$

with S_{pp} defined as the autospectral density and Q_{pp^2} defined as before. Finally, multiplying by $e^{2\alpha r}$ allows the left hand side to be written in terms of a single differential operator

$$\frac{\partial}{\partial r}\left(r^{2m}e^{2\alpha r}S_{pp}\right)=-\frac{\beta\omega}{\rho_0 c_0^3}r^{2m}e^{2\alpha r}Q_{pp^2}, \tag{9}$$

which is identical to Eq. (5) from Morfey and Howell[28] for spherically spreading waves ($m=1$). Equation (9) describes the spatial rate of change in the autospectral density multiplied by a factor of $r^{2m}e^{2\alpha r}$ to correct for losses due to geometric spreading and absorption. The change in this lossless spectrum is due to the nonlinear term on the right of Eq. (9), involving Q_{pp^2}.

B. The change in level due to *Q/S*

Equation (9) may be further manipulated to provide a clearer interpretation of the pressure-squared-pressure quadspectrum term that is independent of the geometric spreading

and absorption. First, the derivative on the left-hand side of Eq. (9) can be expanded through the product rule, the entire equation can be divided by $r^{2m}e^{2\alpha r}S_{pp}$, and terms can be moved to give

$$\frac{1}{S_{pp}}\frac{\partial S_{pp}}{\partial r} = -\frac{2m}{r} - 2\alpha - \frac{\omega\beta p_{\text{rms}}}{\rho_0 c_0^3}\frac{Q}{S}. \tag{10}$$

The right-most term has been multiplied by $p_{\text{rms}}/p_{\text{rms}}$ to express the quadspectrum in a normalized form,

$$\frac{Q}{S} = \frac{Q_{pp^2}(r,f)}{S_{pp}(r,f)p_{\text{rms}}}, \tag{11}$$

which may be viewed as a shape function, independent of amplitude. To further modify Eq. (10), a property of logarithms is used to show

$$\frac{1}{S_{pp}}\frac{\partial S_{pp}}{\partial r} = \frac{\partial}{\partial r}\{\ln(S_{pp})\} = \frac{\partial}{\partial r}\left\{\frac{\log(S_{pp})}{\log(e)}\right\}, \tag{12}$$

where $\log(x)$ denotes $\log_{10}(x)$. Equation (12) can be further manipulated by using the relationship between S_{pp} and the pressure spectrum level,[39] $L_p = 10\log(p^2/p_{\text{ref}}^2) = 10\log(S_{pp}/p_{\text{ref}}^2)$, relative to a reference pressure, p_{ref}:

$$\frac{\log(S_{pp})}{\log(e)} = \frac{1}{\log(e)}\left(\frac{L_p}{10} + 2\log(p_{\text{ref}})\right). \tag{13}$$

This expression can be substituted into Eq. (10) to give

$$\frac{\partial}{\partial r}\left(\frac{L_p}{10} + 2\log(p_{\text{ref}})\right) = \log(e)\left(-\frac{2m}{r} - 2\alpha - \frac{\omega\beta p_{\text{rms}}}{\rho_0 c_0^3}\frac{Q}{S}\right). \tag{14}$$

Since p_{ref} is constant, this becomes

$$\frac{\partial L_p}{\partial r} = -10\log(e)\left(\frac{2m}{r} + 2\alpha + \frac{\omega\beta p_{\text{rms}}}{\rho_0 c_0^3}\frac{Q}{S}\right)$$
$$v(r,\omega) = v_S + v_\alpha + v_N. \tag{15}$$

Equation (15) describes the spatial rate of change in pressure spectrum level, in terms of decibels per meter, as a sum of three effects: geometric spreading, atmospheric absorption, and nonlinearity, which are represented by ν_S, ν_α, and ν_N, respectively. However, the rightmost term involving nonlinearity can be cast in another form using the relations $\omega/c_0 = k$ and $\rho c_0^2 = \gamma p_0$, where p_0 is the ambient atmospheric pressure

$$v_N = -10\log(e)\frac{\omega\beta}{\rho_0 c_0^3}\frac{Q_{pp^2}}{S_{pp}} = -10\log(e)k\frac{\beta}{\gamma}\frac{p_{\text{rms}}}{p_0}\frac{Q}{S}, \tag{16}$$

where $\beta/\gamma = (\gamma+1)/2\gamma$ for an ideal gas. Thus, Eq. (15) may also be expressed as

$$\frac{\partial L_p}{\partial r} = -10\log(e)\left(\frac{2m}{r} + 2\alpha + k\beta M_{\text{rms}}\frac{Q}{S}\right), \tag{17}$$

where M_{rms} is the root-mean-square *acoustic* Mach number, $p_{\text{rms}}/\gamma p_0$. Though the use of M_{rms} is unusual, p_{rms} has been used in the treatment of noise. Both Eq. (15) and Eq. (17) express the spatial rate of change in pressure spectrum level due to nonlinearity as Q/S multiplied by a coefficient. In Eq. (17), the coefficient, $k\beta M_{\text{rms}}$, bears similarity to one definition of the shock formation distance,[40] $\bar{x} = 1/k\beta M$, where M is the acoustic Mach number. This similarity to the shock formation distance is carried further in Sec. II C when discussing initially sinusoidal waveforms, for which the shock formation is well-defined.

Equation (15) and the alternate forms presented in Eq. (16) and Eq. (17) provide quantitative interpretation of the normalized quadspectrum, Q/S, namely, that the spatial rate of change in L_p at a certain location due to nonlinearity is proportional to Q/S. Positive values of Q/S result in a loss of energy and negative values in an increase. Because Q/S is normalized, its values are independent of pressure amplitude and can be thought of as a spectral shape function—two sawtooth waves of the same fundamental frequency but different amplitudes will have the same values of Q/S, but different p_{rms}/p_0. For a given value of Q/S, the spatial rate of change in the pressure spectrum levels scales linearly with frequency and according to the overall gain p_{rms}/p_0. This concept is revisited later in the context of analytical solutions to the GBE. Equation (17) enables a direct, local comparison of the contributions of spreading, absorption, and nonlinearity on a decibel scale to the rate of change of the pressure spectrum level using a single-point measurement.

C. Planar, initially sinusoidal case

The result in Eq. (17) is general and may be applied in any situation where the generalized Burgers equation is valid. However, for the special case of a planar, initially sinusoidal wave a more elegant formulation exists. For a sinusoidal plane wave, the lossless shock formation distance is defined as $\bar{x} = \rho_0 c_0^3/\omega_1\beta\mathcal{P}$, where $\mathcal{P}$ is the amplitude of the initial sinusoid, and ω_1 is its fundamental frequency. The change due to nonlinearity, v_N, from Eq. (16), can be expressed as

$$v_N = -10\log(e)\frac{\omega\beta}{\rho_0 c_0^3}\frac{Q_{pp^2}}{S_{pp}} = -10\log(e)\frac{1}{\bar{x}}\frac{p_{\text{rms}}}{\mathcal{P}\mathcal{P}}\frac{\omega}{\omega_1}\frac{Q}{S}. \tag{18}$$

Since the wave is originally sinusoidal, the only frequencies of interest are the fundamental and its harmonics. In order to differentiate between the sinusoidal and the general case, the following derivations will be presented as $\partial L_n/\partial r$, indicating the change in the nth harmonic. If we assume planar propagation ($m = 0$ and $r = x$), substituting Eq. (18) into Eq. (15) yields the spatial rate of change in L_n as

$$\frac{\partial L_n}{\partial x} = -10\log(e)\left(2\alpha + \frac{1}{\bar{x}}\frac{p_{\text{rms}}}{\mathcal{P}}\frac{\omega_n}{\omega_1}\frac{Q}{S}\right), \tag{19}$$

where $L_n = 20\log(B_n)$ refers to the level, in decibels, of the nth harmonic with normalized amplitude B_n. For a

thermoviscous medium, the absorption for higher harmonics relative to the absorption of the fundamental frequency is $\alpha = \alpha_1(\omega_n/\omega_1)^2 = \alpha_1 n^2$, with α_1 equal to the absorption at the fundamental frequency and n the order of the harmonic. After this substitution and multiplication of Eq. (19) by $\bar{x}$, the spatial rate of change of the level of the nth harmonic relative to the normalized distance $\sigma = x/\bar{x}$ is given by

$$\frac{\partial L_n}{\partial \sigma} = -10\log(e)\left(\frac{2}{\Gamma}n^2 + n\frac{p_{\rm rms}}{\mathcal{P}}\frac{Q}{S}\right)$$
$$\nu(\sigma, n) = \nu_\alpha + \nu_N, \tag{20}$$

where $\Gamma = 1/\bar{x}\alpha_1$ is the well-known Gol'dberg number, comparing the strength of nonlinearity with that of atmospheric absorption. Equation (20) is valid for planar propagation of initially sinusoidal waveforms, such as analytical solutions to the GBE and within plane wave tubes. This nondimensional form of Eq. (17) is useful in developing a quantitative understanding of how Q/S is related to the spatial rate of change in the levels of the harmonic components analytical examples in Sec. III.

III. COMPARISON WITH SOLUTIONS TO THE GBE

To test the validity of Eq. (20), the evolution of $\nu(\sigma, n)$ in terms of ν_α and ν_N is compared with what is traditionally obtained for known solutions of the GBE for an initially sinusoidal plane wave. The two solutions that are considered in this paper are the Blackstock Bridging Function[41] (BBF) and the Mendousse[42] solution. In contrast with other solutions, such as the Fubini[43] and Fay[44] solutions, these two solutions are valid for all values of σ, making them ideal candidates for such a comparison. The following comparisons will show the spatial rate of change in the level of the nth harmonic calculated via two distinct methods. First, numerical derivatives, with respect to distance, of the amplitude B_n show how the spectrum evolves analytically according to the GBE and are referred to as actual changes in Sec. III A and III B. The second method uses Eq. (20) to predict the spatial rate of change in level for the same harmonics. Specifically, the waveforms are calculated according to the BBF or the Mendousse solution, following which the Fourier transforms of the pressure and pressure-squared waveforms are used to calculate Q/S. The results of Eq. (20) are referred to as predicted changes in Sec. III A and III B. The agreement between the actual and predicted changes shows that the normalized quadspectrum Q/S calculated for a waveform may be used as a single-point measurement to accurately estimate the spatial rate of changes due to nonlinearity on a decibel scale.

A. BBF

The BBF[41] was originally presented to bridge the gap between the Fubini solution, valid before the shock formation distance, and the Fay solution, valid in the sawtooth regime. It represents a lossless ($\Gamma \to \infty$) wave propagating nonlinearly and is dependent only on the initial amplitude p_0 and the normalized distance σ. The pressure waveform, p, as a function of retarded time τ is expressed in terms of the infinite sum

$$\frac{p}{\mathcal{P}} = \sum_{n=1}^{\infty} B_n \sin(\omega_n \tau), \tag{21}$$

where the amplitude of the nth harmonic is

$$B_n = \frac{2}{n\pi}V_b + \frac{2}{n\pi\sigma}\int_{\Phi_{\rm min}}^{\pi} \cos\{n[\Phi - \sigma\sin(\Phi)]\}d\Phi, \tag{22}$$

and V_b and $\Phi_{\rm min}$ are solutions to transcendental equations given by Blackstock.[41] Figure 1(a) shows example waveforms at distances of $\sigma = 0$ to 3 in steps of 0.5. The distances $\sigma = 0$, 1, and 3 represent the origin, shock formation distance, and what is the traditionally regarded as the onset of the sawtooth regime, respectively. Figure 1(b) shows the amplitude of the coefficients B_n as a function of σ, for $n = 1$, 2, 5, 10, and 20, the last few being of higher order than those

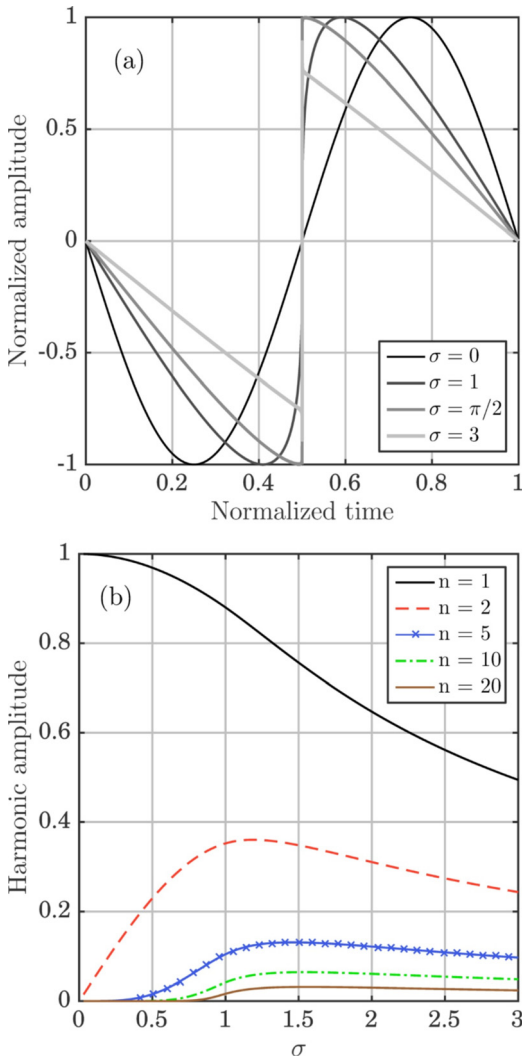

FIG. 1. (Color online) (a) The pressure waveforms for the Blackstock Bridging Function plotted at normalized distances of $\sigma = 0$ to 3 in steps of 0.5. (b) The harmonic amplitudes, B_n, plotted on a linear scale vs σ for $n = 1$, 2, 5, 10, and 20. In order to accurately characterize the waveforms and reliably capture the higher harmonics, 12 000 terms are needed in Eq. (21) with a sampling rate of 24 000 samples per period.

shown originally by Blackstock.[41] Figure 1 provides a reference to better understand the spatial rate of change in the harmonic amplitudes, which is the foundation for one method of calculating $\partial L_n/\partial\sigma$.

While Fig. 1(b) presents a traditional view of normalized harmonics amplitudes, the current formulation provides a link between the spatial rate of change in the normalized spectral amplitudes, $S_n = B_n^2$, for the evolution of an initial sinusoid waveform, described in this case by the BBF, and the normalized quadspectrum, Q/S. The actual changes in S_n with distance [obtained from the B_n shown in Fig. 1(b)] are depicted as circles in Fig. 2, and the accompanying lines show the predicted changes from Eq. (20) using Q/S from the Fourier transform of the waveforms calculated using Eq. (21), with an adequate number of terms to accurately described the sharp discontinuity. For the cases shown here, 12 000 terms in the infinite series in Eq. (21) were used with a sampling rate of 24 000 samples/period. With the exception of the decreasing amplitude of the first harmonic, the amplitude of each of the other harmonics initially increases. At $\sigma = \pi/2$, the discontinuity reaches a maximum amplitude. After this point, all of the harmonics decrease in amplitude, which corresponds to a negative $\partial S_n/\partial\sigma$.

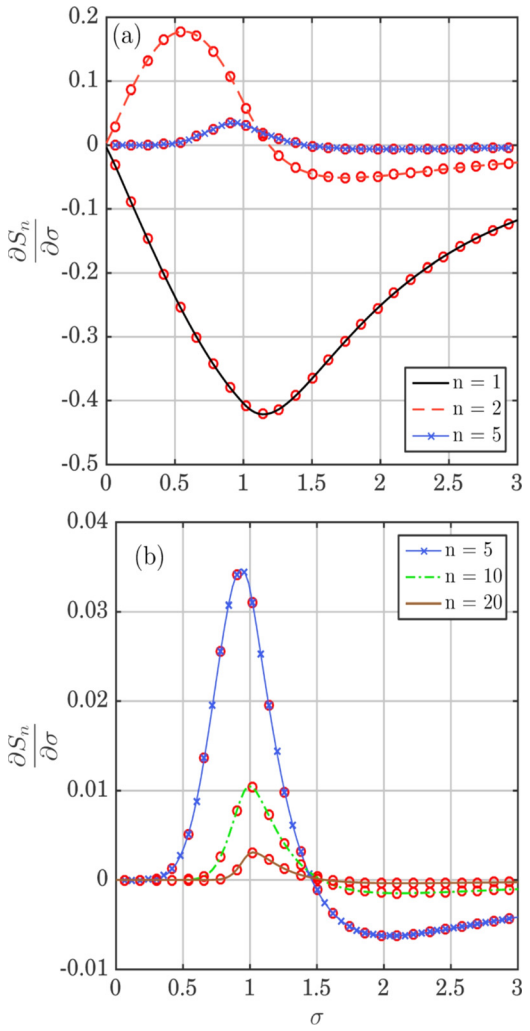

FIG. 2. (Color online) The predicted (lines) and actual (circles) rate of change in the normalized spectral amplitudes, S_n, with respect to the normalized distance σ for harmonic numbers (a) $n = 1$, 2, 5 and (b) $n = 5$, 10, 20. Predicted values are calculated using Eq. (20), while the actual changes are calculated via a numerical derivative of the calculated BBF coefficients for each harmonic with respect to σ. Waveforms and harmonic amplitudes have been generated using the same number of terms and sampling frequency as Fig. 1.

The spatial rate of change in the normalized levels, L_n, predicted in Eq. (20) is connected to the changes displayed in Fig. 2, but as levels are logarithmic quantities, the connection between the two can be difficult to see. In order to aid in forming this association, Fig. 3 shows the normalized spectrum, $S_n = B_n^2$, plotted on a logarithmic scale in the y axis. The amplitude of the first harmonic still begins at one and decreases with σ, while all of the other harmonics are originally at zero amplitude before increasing and then decreasing in amplitude. The slope of the lines plotted on this logarithmic scale resembles the spatial rate of change in L_n predicted using $\nu(\sigma, n)$ in Eq. (20). For $\sigma > \pi/2$, the lines of each of the harmonics appear to approach the same slope such that the rate of change in level is similar across all harmonics in the sawtooth region, an important point that is emphasized in comparing Q/S calculations for various harmonics.

Figure 4 shows the actual spatial rate of change in $L_n = 10\log S_n$ as circles and the changes found using $\nu(\sigma, n)$ as patterned lines. Because the BBF neglects absorption, $\Gamma \to \infty$ and all of the predicted changes seen in Fig. 4 are due to nonlinearity: $\nu(\sigma, n) = \nu_N$. The actual change in L_n is obtained by differentiating $L_n = 20\log(\mathrm{p}/\mathrm{p}_{\mathrm{ref}})$ with respect to σ

$$\begin{aligned}\frac{\partial L_n}{\partial\sigma} &= 20\frac{\partial}{\partial\sigma}\left(\log(B_n) - \log(p_{ref})\right)\\ &= 20\frac{\partial}{\partial\sigma}\frac{\ln(B_n)}{\ln(10)}\\ &= 20\log(e)\frac{1}{B_n}\frac{\partial B_n}{\partial\sigma}.\end{aligned} \tag{23}$$

Because harmonics with $n > 1$ originally have zero amplitude, the initial spatial rate of change in level is infinite and

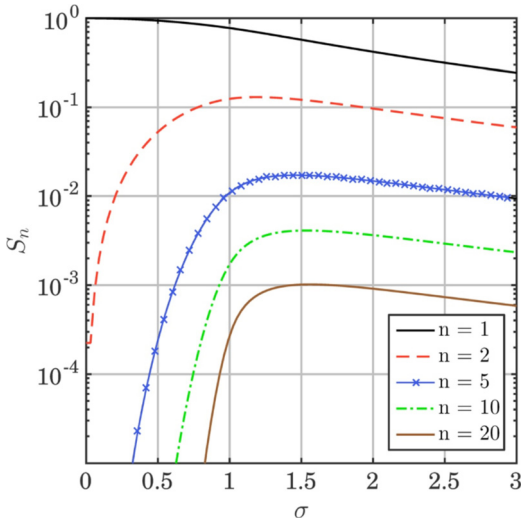

FIG. 3. (Color online) Normalized spectral amplitudes, S_n, for the harmonics shown in Fig. 1(b) plotted on a logarithmic scale.

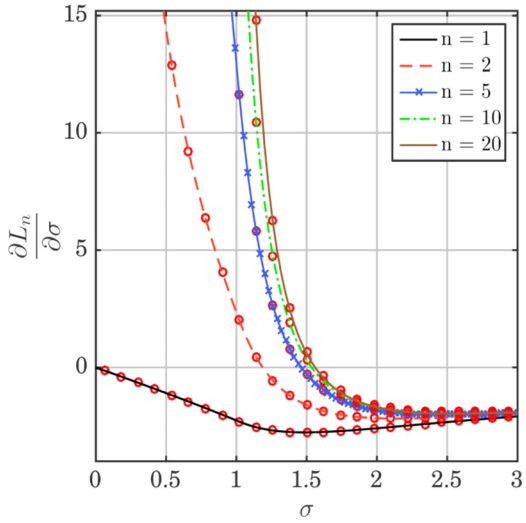

FIG. 4. (Color online) The spatial rate of change in the level L_n for harmonics $n = 1$, 2, 5, 10, and 20 for the BBF as a function of σ. The patterned lines represent the predicted changes due to nonlinearity, based on the normalized quadspectrum, and the circles represent the actual change in harmonic level. Waveforms and spectral amplitudes are generated using the same number of terms and sampling rate as Fig. 1.

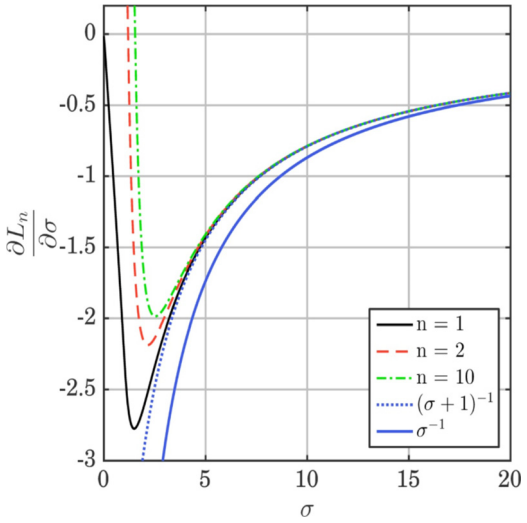

FIG. 5. (Color online) The spatial rate of change in L_n as predicted using the quadspectrum in Eq. (20) for $n = 1$, 2, and 10 is compared with the changes predicted using Eq. (25) and Eq. (26), where the decay is proportional to $(\sigma+1)^{-1}$ and σ^{-1}, respectively. The decay rates of all harmonics converge as the wave enters the sawtooth region ($\sigma > 3$), and for $\sigma \gg 1$ the decay of all harmonics agrees with the approximation of Eq. (26). Waveforms and spectral amplitudes were generated using the same number of terms as Fig. 1.

decreases with increasing distance. Excellent agreement can be seen between the two calculations for $\partial L_n/\partial\sigma$, confirming the ability of Q/S in Eq. (20) to quantify the changes due to nonlinearity for the case of no absorption. In addition, the regions of shock formation and decay are easily distinguished. For sinusoidal signals, when the shock is forming and growing, higher harmonics have positive rate of change in level due to nonlinearity, corresponding to a negative value of Q/S. However, as the shock decays, all of the harmonics have a negative rate of change and Q/S is positive. As the shock enters the sawtooth region, the decay rate of all of the harmonics begins to converge.

The converging behavior for the harmonic decay can be compared with established nonlinear behavior in the sawtooth region to help describe the asymptotic behavior of Q/S. Blackstock *et al.*[45] show that in this region, the amplitudes of all of the harmonics decay as

$$B_n = \frac{2}{(\sigma+1)n}. \tag{24}$$

Using Eq. (23), the corresponding asymptotic change in L_n is

$$\frac{\partial L_n}{\partial \sigma} = 20\log(e)\left(-\frac{1}{\sigma+1}\right). \tag{25}$$

A comparison of this expression, which is valid for all harmonics in the sawtooth region, and the behavior predicted by Eq. (20) is shown over a longer distance in Fig. 5 for harmonics $n = 1$, 2, 10. The comparison shows that Eq. (25) provides a reasonable estimate to the actual rate of change of the harmonic levels in the sawtooth region. In this region, the levels of the harmonics are not only all decaying, but are all decaying at the same rate.

The limiting behavior in the spatial range of change of the levels associated with the spectral amplitudes for all harmonics can be compared with theory for acoustic saturation. The concept of acoustic saturation states that for $\sigma \gg 1$, the amplitude of the pressure waveform depends only on the distance the wave has traveled, x, and is irrespective of initial amplitude, p_0. For $\sigma \gg 1$, an approximation can be made in Eq. (25) that $\sigma + 1 \cong \sigma$, which is plotted as a solid line in Fig. 5 for comparison. Because acoustic saturation is typically described in terms of x, the substitution $\sigma = x/\bar{x}$ is made into Eq. (25) to give an asymptotic relationship for the spatial rate of change in the harmonic levels for lossless, planar propagation

$$\frac{\partial L_n}{\partial x} = \nu_N = -20\log(e)\frac{1}{x}. \tag{26}$$

This decay proportional to $1/x$ is in agreement with expected behavior from Eq. (20). As the wave propagates in the sawtooth regime, Q/S remains constant, meaning the only variable changing is p_{rms}, which changes proportional to $1/x$.

The regime of acoustic saturation was investigated experimentally by Webster and Blackstock[46] who found that the spatial rate of change in level of the harmonics at large distances is independent of the source amplitude. In this way, the principle of acoustic saturation can be seen to agree with the changes calculate using Q/S values of the BBF.

B. The Mendousse solution

The second analytical solution that provides support for the quantitative evaluation of Q/S is the Mendouse solution, which, like the BBF, is an infinite sum describing the propagation of an initially sinusoidal wave.[42] However, in contrast with the BBF, the Mendousse solution takes into account thermoviscous absorption, such that both ν_α and ν_N must be calculated and summed together to yield the total spatial rate of change in L_n.

In the infinite sum of the Mendousse solution, the presence of atmospheric absorption is indicated by the presence of the Gol'dberg number, Γ:

$$\frac{p}{\mathcal{P}}=\frac{\frac{4}{\Gamma}\sum_{n=1}^{\infty}(-1)^{n+1}I_n\left(\frac{\Gamma}{2}\right)ne^{-n^2\sigma/\Gamma}\sin(\omega_n\tau)}{I_0\left(\frac{\Gamma}{2}\right)+2\sum_{n=1}^{\infty}(-1)^nI_n\left(\frac{\Gamma}{2}\right)e^{-n^2\sigma/\Gamma}\cos(\omega_n\tau)}. \quad (27)$$

In the limit that $\Gamma\to\infty$, the Mendousse solution will give the same results as the BBF. For finite Γ, the Mendousse solution exhibits behavior similar to the BBF, but the wave decays at a faster rate due to the presence of absorption. For lower amplitudes of Γ, the absorption may prevent the formation of a sawtooth wave. Figure 6(a) shows a comparison of waveforms generated with the BBF and the Mendousse solution for $\Gamma=30$ at $\sigma=\pi/2$. The Mendousse waveform has decayed slightly in amplitude, and the shock is significantly less sharp than that calculated using the BBF.

The spatial rate of change in L_n for the harmonics $n=1$, 2, 5, 10, and 20 are displayed in Figs. 6(b)–6(f) as a function of σ. The terms ν_α, rate of change due to atmospheric absorption, and ν_N, rate of change due to nonlinearity via Q/S [see Eq. (20)], are shown as dash and dash-dot lines, respectively. The total rate of change, $\partial L_n/\partial\sigma=\nu=\nu_\alpha+\nu_N$ (solid line) is compared with the actual change in

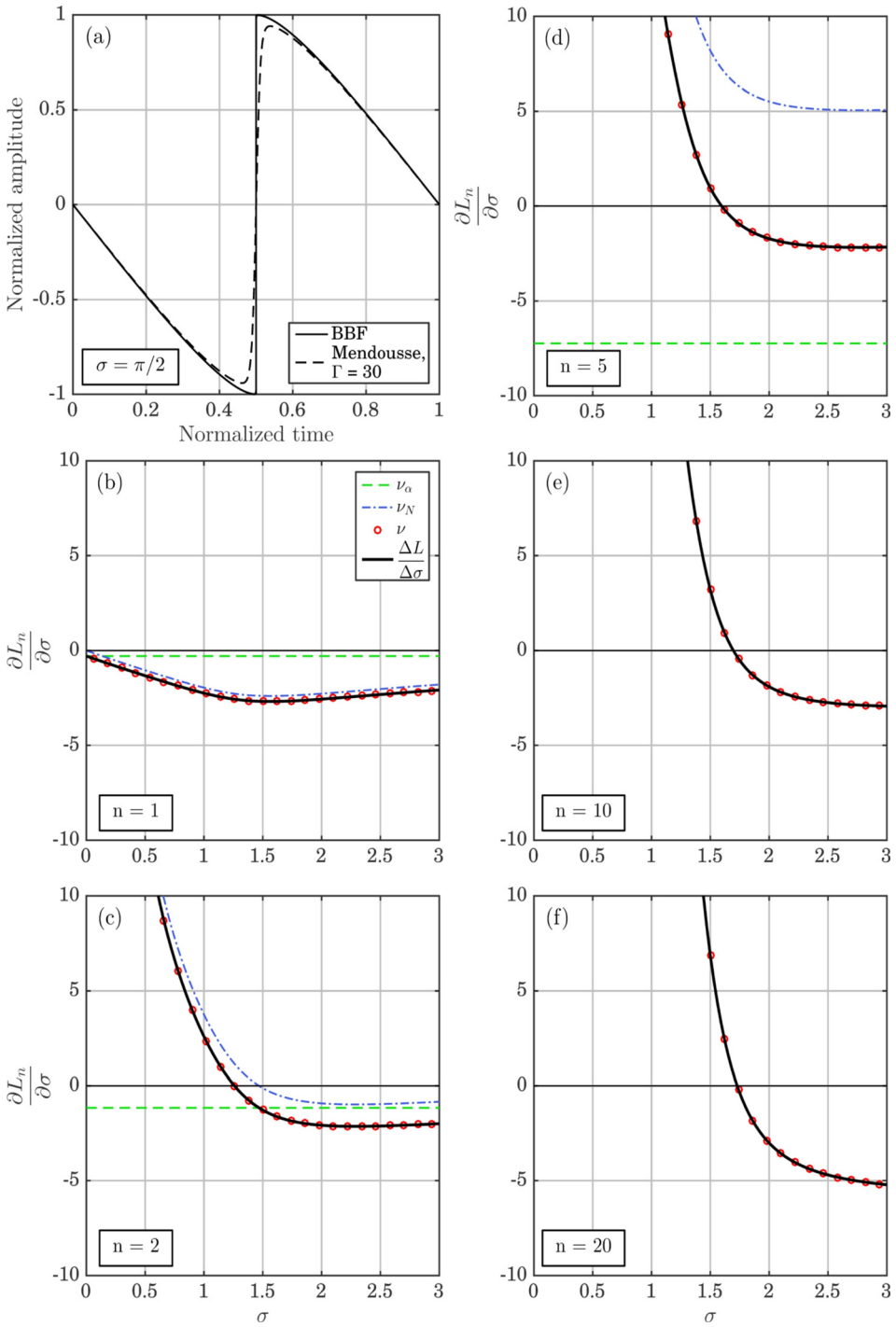

FIG. 6. (Color online) (a) A waveform of the Mendousse solution is compared with the BBF at $\sigma=\pi/2$ and $\Gamma=30$. (b)–(f) The spatial rate of change in level for harmonics $n=1$, 2, 5, 10, and 20. The spatial rate of change due to absorption, ν_α, nonlinearity, ν_N, and their sum, ν, are shown by dashed, dashed-dot, and solid lines, respectively. The actual changes in harmonic levels are shown as circles that overlay the solid lines. For $n=10$ and 20 [shown in (e) and (f)], ν_α and ν_N both lie outside the plotted range. For the specified value of $\Gamma=30$, the absorption for $n=10$ is constant at $-28.95\,\mathrm{dB}/\sigma$, and for $n=20$ it is $-115.8\,\mathrm{dB}/\sigma$. 200 terms were used in both the numerator and denominator of the Mendousse solution, at a sampling rate of 400 samples per period.

the level of the harmonics with respect to σ. To generate the waveforms in this example using Eq. (27), 200 terms are needed in both the numerator and the denominator of Eq. (27) at a sampling rate of 400 samples per wavelength. Because the Mendousse solution does not produce as steep a waveform as the BBF, the number of terms required to accurately characterize each waveform is significantly less. The coefficients B_n do not have a compact analytical form, as is the case of the BBF, because of the time-dependent infinite sum in the denominator. Hence, the levels, L_n, and corresponding numerical derivatives of L_n with respect to σ are obtained using Fourier transforms of the waveforms. There is excellent agreement between these numerical derivatives (circles) and the rate of change based on Q/S.

Trends can be seen in examining the spatial rate of change in harmonic levels for the Mendousse solution [Figs. 6(b)–6(f)]. Initially, an infinite rate of change in level is observed for all of the harmonics except $n = 1$, for the same reasons as in the BBF case. The rate of change due to nonlinearity, ν_N, is much larger than that due to absorption, ν_α, during shock formation and growth. As the shock propagates, the magnitude of the rate of change due to nonlinearity approaches the same order of magnitude as from absorption. However, at greater σ, the absorption dominates and $\partial L_n/\partial\sigma < 0$, indicating the harmonics are decreasing in amplitude. Because a true discontinuity does not form for this value of Γ, nonlinear losses due to weak shock theory are absent, the waveform continues to steepen, and ν_N remains positive over a larger distance than is seen for the BBF. In addition, for higher harmonics the distance at which the total spatial rate of change goes negative is slightly delayed from the distance of $\sigma = \pi/2$ seen in the BBF. This change is due to a slower wave steepening process in the presence of absorption. Thus, the distance at which the rate of change goes negative varies both between the inviscid case and the thermoviscous case, and with increasing n.

Important trends can be seen when comparing results from the Mendousse solution with those from the BBF. In both cases excellent agreement is seen between numerical derivatives calculated using the spectral amplitudes and the rate of change found using Q/S via Eq. (20). In addition, the same general principles apply with regard to the development of shocks: positive values of ν for higher harmonics indicate the formation of shocks, while negative values of ν across all harmonics indicates shock decay. However, important differences arise. In the inviscid case, nonlinear losses due to weak shock theory are present, resulting in negative values of ν_N. In contract, when absorption is high enough that a true discontinuity never forms, the absorption is explicitly separated as ν_α, and ν_N remains positive. Another important case is that shock formation is delayed in the thermoviscous case when compared with the inviscid case due to the presence of absorption. Despite these differences, similar behavior in the total change ν enables a comparison of trends observed in both cases.

IV. CONCLUSION

The derivation of the power spectrum-based formulation of the GBE presented by Morfey and Howell[28] has been carried farther to yield the spatial rate of change of pressure spectrum level of an arbitrary waveform. This further derivation enables a single-point measurement capable of directly comparing and differentiating between the effects of nonlinearity, absorption, and geometric spreading in a decibel sense. This formulation of the GBE has been applied to two analytical solutions to the GBE for initially sinusoidal waveforms, an inviscid and thermoviscous. In both cases, the total spatial rate of change of the harmonic level, ν, calculated using Q/S agrees with the actual changes in the levels calculated in the waveforms. In addition, certain trends can be observed in both cases. For both the lossless and the lossy initially sinusoidal cases, positive values of ν across all higher harmonics indicate waveform steepening. In contrast, negative values of ν across all frequencies indicate that the maximum shock steepness for that scenario has been reached and harmonic levels are decaying. Decay at the same rate indicates the weak-shock regime is maintained; however, if ν is increasingly negative at higher frequencies, the waveform shock retains a finite thickness.

This paper has shed significant quantitative insight on the meaning of Q/S as a nonlinearity indicator, but with the primary motivation for the investigation being the understanding the role of nonlinearity jet and rocket noise spectral evolution. Important differences exist between geometrically spreading broadband noise and initial planar sinusoids, such as different parts of the waveform steepening at different rates. Prior studies[2,6] involving Q/S have indicated that both positive and negative portions of the nonlinear normalized spectral shape exist. Future quadspectrum-based analyses of these noise fields will apply the mathematical theory of separating the power spectrum spatial rate of change into geometric, absorptive, and nonlinear components, as well as incorporate an understanding of the limiting weak-shock behavior described here as a function of frequency and range.

ACKNOWLEDGMENTS

The authors would like to gratefully acknowledge the funding for this work, in part by a grant from the Office of Naval Research, with Joseph Doychak as program manager, and in part by an appointment of B.O.R. to the Student Research Participation Program at the U.S. Air Force Research Laboratory, 711th Human Performance Wing, Human Effectiveness Directorate, Warfighter Interface Division, Battlespace Acoustics Branch administered by the Oak Ridge Institute for Science and Education through an interagency agreement between the U.S. Department of Energy and USAFRL.

[1]S. A. McInerny, "Launch vehicle acoustics Part 2: Statistics of the time domain data," J. Aircraft **33**, 518–523 (1996).
[2]S. A. McInerny and S. M. Ölçmen, "High-intensity rocket noise: Nonlinear propagation, atmospheric absorption, and characterization," J. Acoust. Soc. Am. **117**, 578–591 (2005).
[3]K. L. Gee, R. J. Kenny, T. B. Neilsen, T. W. Jerome, C. M. Hobbs, and M. M. James, "Spectral and statistical analysis of noise from reusable solid rocket motors," Proc. Mtgs. Acoust. **18**, 040002 (2013).

[4]B. Greska and A. Krothapalli, "On the far-field propagation of high-speed jet noise," in *Proceedings of NCAD2008* (2008), Paper No. NCAD2008-73071.
[5]S. A. McInerny, M. Downing, C. Hobbs, and M. Hannon, "Metrics that characterize nonlinearity in jet noise," AIP Conf. Proc. **838**, 560–563 (2006).
[6]K. L. Gee, T. B. Gabrielson, A. A. Atchley, and V. W. Sparrow, "Preliminary analysis of nonlinearity in military jet aircraft noise propagation," AIAA J. **43**, 1398–1401 (2005).
[7]K. L. Gee, T. B. Neilsen, M. B. Muhlestein, A. T. Wall, J. M. Downing, and M. M. James, "On the evolution of crackle in jet noise from high-performance engines," in *19th AIAA/CEAS Aeroacoustics Conference* (2013), AIAA Paper No. 2013-2190.
[8]J. A. Gallagher and D. K. McLaughlin, "Experiments on the non-linear characteristics of noise propagation from low and moderate Reynolds number supersonic jets," in *7th Aeroacoustics Conference* (1981), AIAA Paper No. 81-2041.
[9]B. P. Petitjean, K. Viswanathan, and D. K. McLaughlin, "Acoustic pressure waveforms measured in high speed jet noise experiencing nonlinear propagation," Int. J. Aeroacoust. **5**, 193–215 (2006).
[10]P. Mora, N. Heeb, J. Kastner, E. J. Gutmark, and K. Kailasanath, "Near and far field pressure skewness and kurtosis in heated supersonic jets from round and chevron nozzles," in *Proceedings ASME Turbo Expo* (June 2013), Paper No. GT2013-95774.
[11]N. Cacqueray and C. Bogey, "Noise of an overexpanded Mach 3.3 jet: Non-linear propagation effects and correlations with flow," Int. J. Aeroacoust. **13**(7), 607–632 (2014).
[12]K. L. Gee, T. B. Neilsen, and A. A. Atchley, "Skewness and shock formation in laboratory-scale supersonic jet data," J. Acoust. Soc. Am. **133**, EL491–EL497 (2013).
[13]W. J. Baars, C. E. Tinney, M. S. Wochner, and M. F. Hamilton, "On cumulative nonlinear acoustic waveform distortions from high-speed jets," J. Fluid Mech. **749**, 331–366 (2014).
[14]R. Fievet, C. E. Tinney, W. J. Baars, and M. F. Hamilton, "Acoustic waveforms produced by a laboratory scale supersonic jet," in *20th AIAA/CEAS Aeroacoustics Conference* (2014), AIAA Paper No. 2014-2907.
[15]K. L. Gee, T. B. Neilsen, B. O. Reichman, M. B. Muhlestein, D. C. Thomas, J. M. Downing, M. M. James, and R. L. McKinley, "Comparison of two time-domain measures of nonlinearity in near-field propagation of high-power jet noise," in *20th AIAA/CEAS Aeroacoustics Conference* (2014), AIAA Paper No. 2014-3199.
[16]M. B. Muhlestein, K. L. Gee, T. B. Neilsen, and D. C. Thomas, "Evolution of the average steepening factor for nonlinearly propagating waves," J. Acoust. Soc. Am. **137**, 640–650 (2015).
[17]B. O. Reichman, M. B. Muhlestein, K. L. Gee, T. B. Neilsen, and D. C. Thomas, "Evolution of the derivative skewness for nonlinearly propagating waves," J. Acoust. Soc. Am. **139**(3), 1390–1403 (2016).
[18]Y. C. Kim and E. J. Powers, "Digital bispectral analysis and its applications to nonlinear wave interactions," IEEE Trans. Plasma Sci. **7**, 120–131 (1979).
[19]S. N. Gurbatov, A. N. Malakhov, and N. V. Pronchatov-Rubtsov, "Evolution of higher-order spectra of nonlinear random waves," Radiophys. Quantum Electron. **29**, 523–528 (1986).
[20]S. N. Gurbatov, A. N. Malakhov, and N. V. Pronchatov-Rubtsov, "Application of higher-order spectra in problems of the diagnosis of strong acoustic noise," Sov. Phys. Acoust. **33**(5), 549–550 (1987).
[21]K. Sakamagi, S. Aoki, I. M. Chou, T. Kamakura, and K. Ikegaya, "Statistical characteristics of finite amplitude acoustic noise propagating in a tube," J. Acoust. Soc. Jpn. **3**, 43–45 (1982).
[22]K. L. Gee, A. A. Atchley, L. E. Falco, T. B. Gabrielson, and V. W. Sparrow, "Bispectral analysis of high-amplitude jet noise," in *11th AIAA/CEAS Aeroacoustics Conference* (2005), Paper No. AIAA-2005-2937.
[23]K. L. Gee, A. A. Atchley, L. E. Falco, M. R. Shepherd, L. S. Ukeiley, B. J. Jansen, and J. M. Seiner, "Bicoherence analysis of model-scale jet noise," J. Acoust. Soc. Am. **128**, EL211–EL216 (2010).
[24]D. E. Gagnon, "Bispectral analysis of nonlinear acoustic propagation," M.S. thesis, University Texas, Austin, TX, 2011.
[25]J. S. Bendat and A. G. Piersol, *Engineering Application of Correlation and Spectral Analysis* (Wiley-Interscience, New York, 1980), 55 pp.
[26]In previous papers this quantity has been called both Q_{pp^2} and Q_{p^2p}. This paper will follow the nomenclature given in Bendat and Piersol (Ref. 27), that Q_{pp^2} implies that the complex conjugate of $\tilde{p}$ is taken rather than that of p^2.
[27]J. S. Bendat and A. G. Piersol, *Random Data: Analysis and Measurement Procedures* (John Wiley and Sons, Hoboken, NJ, 2010), Chap. 5, p. 127.
[28]C. L. Morfey and G. P. Howell, "Nonlinear propagation of aircraft noise in the atmosphere," AIAA J. **19**, 986–992 (1981).
[29]Y. Nagata, "Lag joint probability, higher order covariance function and higher order spectrum," La Mer **8**, 78–94 (1970).
[30]Y. Nagata, "Bispectra of spike-array type time series and their application to the analysis of oceanic microstructures," J. Oceanographical Soc. Jpn. **34**, 204–216 (1978).
[31]S. A. McInerny, K. L. Gee, J. M. Downing, and M. M. James, "Acoustical nonlinearities in aircraft flyover data," in *13th AIAA/CEAS Aeroacoustics Conference* (2007), AIAA Paper No. 2007-3654.
[32]W. J. Baars, C. E. Tinney, and M. S. Wochner, "Nonlinear noise propagation from a fully expanded mach 3 jet," in *50th AIAA Aerospace Sciences Meeting including the New Horizons Forum and Aerospace Exposition* (2012), AIAA Paper No. 2012-1177.
[33]H. Lee, T. Park, W. S. Ohm, and D. Lee, "Jet noise-based diagnosis of combustion instability in solid rocket motors," J. Acoust. Soc. Am. **136**, 2137 (2014).
[34]J. M. Downing, K. L. Gee, S. A. McInerny, T. B. Neilsen, and M. M. James, "Do recent findings on jet noise answer aspects of the Schultz curve?" Proc. Mtgs. Acoust. **19** 040022 (2013).
[35]L. E. Falco, "Single-point nonlinearity indicators for the propagation of high-amplitude acoustic signals," Ph.D. dissertation, The Pennsylvania State University, State College, PA, 2007.
[36]L. E. Falco, A. A. Atchley, K. L. Gee, and V. W. Sparrow, "Investigation of a single-point nonlinearity indicator in one-dimensional propagation," AIP Conf. Proc. **838**, 572 (2006).
[37]L. E. Falco, A. A. Atchley, and K. L. Gee, "Investigation of a single-point nonlinearity indicator in the propagation of high-amplitude jet noise," in *12th AIAA/CEAS Aeroacoustics Conference* (2006), AIAA Paper No. 2006-2529.
[38]R. O. Cleveland, M. F. Hamilton, and D. T. Blackstock, "Time-domain modeling of finite-amplitude sound in relaxing fluids," J. Acoust. Soc. Am. **99**(6), 3312–3318 (1996).
[39]L. E. Kinsler, A. R. Frey, A. B. Coppens, and J. V. Sanders, *Fundamentals of Acoustics* (Wiley, Hoboken, NJ, 1999), Chap. 5, 130 pp.
[40]D. T. Blackstock, "History of nonlinear acoustics: 1750s-1930s," in *Nonlinear Acoustics*, edited by M. F. Hamilton and D. T. Blackstock (Academic Press, San Diego, 1998), Chap. 1, 15 pp.
[41]D. T. Blackstock, "Connection between the Fay and Fubini solutions for plane sound waves of finite amplitude," J. Acoust. Soc. Am. **39**, 1019–1026 (1966).
[42]J. S. Mendousse, "Nonlinear dissipative distortion of progressive sound waves at moderate amplitudes," J. Acoust. Soc. Am. **25**, 51–54 (1953).
[43]E. Fubini, "Anomalie nella propagazione di ande acustiche de grande apiezza" ("Anomalies in acoustic wave propagation of large amplitude"), Alta Frequenza **4**, 530–581 (1935) [English translation: R. T. Beyer, Nonlinear Underwater Sound, 118–177 (1984)].
[44]R. D. Fay, "Plane sound waves of finite amplitude," J. Acoust. Soc. Am. **3**, 222–241 (1931).
[45]D. T. Blackstock, M. F. Hamilton, and A. D. Pierce, "Progressive waves in lossless and lossy fluids," in *Nonlinear Acoustics*, edited by M. F. Hamilton and D. T. Blackstock (Academic Press, San Diego, 1998), Chap. 4, p. 116.
[46]D. A. Webster and D. T. Blackstock, "Finite-amplitude saturation of plane sound waves in air," J. Acoust. Soc. Am. **62**, 518–523 (1977).